Ecological Informatics 81 (2024) 102590

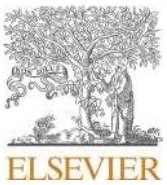

Contents lists available at ScienceDirect

Ecological Informatics

journal homepage: www.elsevier.com/locate/ecolinf

First woody cover vegetation map of Kruger National Park in 1939–1944: Evidence from historical black and white aerial photography

Tullia Riccardi [a,*], Benjamin J. Wigley [b,c,d], Linda Kleyn [e], Corli Coetsee [c,d], Sandra MacFadyen [f,g], Fabio Attorre [a], Luca Malatesta [a]

[a] Department of Environmental Biology, Sapienza University of Rome, Piazzale Aldo Moro 5, 00185 Rome, Italy
[b] Plant Ecology, University of Bayreuth, Universitätsstr. 30, Bayreuth 95440, Germany
[c] School of Natural Resource Management, Nelson Mandela University, George 6529, South Africa
[d] Scientific Services, Kruger National Park, Private Bag X402, Skukuza 1350, South Africa
[e] Spesfeed Consulting, P O Box 955, Broederstroom, 0240 Northwest, South Africa
[f] Mathematical Biosciences, Department of Mathematical Sciences, Stellenbosch University, Stellenbosch 7602, South Africa
[g] National Institute for Theoretical and Computational Sciences, Stellenbosch University, 7602, South Africa

ARTICLE INFO

Keywords:
Savanna ecosystem
Vegetation mapping
Object-based image analysis (OBIA)
Google earth engine (GEE)
Random forest
Historical baseline

ABSTRACT

Long-term spatial studies are crucial for understanding how the Earth's surface has changed. Before satellite imagery, landscapes were monitored using black and white (B&W) aerial photographs. However, surveys were infrequent and image analysis was a manual process that was both time-consuming and costly. In this study, we created a composite of high spatial resolution (0.5–0.75 m) B&W aerial images from 1939–1944, covering about 91% of Kruger National Park (KNP)'s nearly 2 million ha. We used this to produce the first historical woody cover (tall trees and shrubs) map of KNP, which until now was only partially understood through fragmented descriptions in period literature and small-area case studies. We established a supervised learning workflow using Google Earth Engine (GEE) which included performing an Object-based Image Analysis (OBIA) with a Random Forest classifier. This approach, enhanced by integrating texture, shape, neighboring features, and spectral variables into the training/validation dataset, enabled the identification of woody vegetation from B&W landscape objects. To enhance accuracy, we guided our sampling method using vegetation types with comparable woody cover and species composition. Initially, we tested our method on a smaller set of images (25 km^2), and after confirming its effectiveness, we then expanded the approach to cover all available historical aerial imagery. Our results show that in 1939–1944, 26% of KNP was covered in woody vegetation (overall accuracy of 89%, producer's accuracy (non-woody = 88%, woody = 90%), and user's accuracy (non-woody = 90%, woody = 87%)). The importance of geological substrate in driving vegetation pattern is reflected in a higher woody cover percentage on granite (28%) than on basalt (21%) soils, with the lowest woody cover on northern basalts (11%) and the highest on north-central granites (32%). This study highlights the potential of GEE and OBIA for analyzing large-area, high spatial resolution B&W aerial photographs in a systematic and efficient manner and the importance of creating large-scale historical land cover baselines to support environmental planning and landscape management.

1. Introduction

The Earth's surface is rapidly changing and concerns over climate change, habitat loss and fragmentation, food security, and natural resource exploitation are increasing (Alves de Oliveira et al., 2021; Godfray et al., 2010; Powers and Jetz, 2019; United Nations Convention to Combat Desertification, 2022). Monitoring how a landscape changes through time is a crucial element for ecological management, environmental planning, and improving conservation efforts (Hassan et al., 2016; Tassi and Vizzari, 2020; Vogels et al., 2017). Although freely available satellite imagery has made remote sensing a powerful, cost-effective, and widespread tool, the oldest satellite images are from the early 1970s, which limits our knowledge of how natural landscapes used to look and how they have changed over longer time periods. The

* Corresponding author.
E-mail address: tullia.riccardi@uniroma1.it (T. Riccardi).

https://doi.org/10.1016/j.ecoinf.2024.102590
Received 24 October 2023; Received in revised form 24 March 2024; Accepted 5 April 2024
Available online 8 April 2024
1574-9541/© 2024 The Authors. Published by Elsevier B.V. This is an open access article under the CC BY license (http://creativecommons.org/licenses/by/4.0/).

absence of past information and historical datasets increases the establishment of inappropriate baselines for nature conservation, restoration, and management policies (Soga and Gaston, 2018).

Prior to satellite imagery, high spatial resolution black and white (B&W) aerial photography was used to map land cover and soils (Bauer, 1975; Wright, 1973). Munteanu et al. (2020) also highlight the Corona spy satellite, in operation from 1960 to 1972, for high spatial resolution imagery as a resource for long-term studies on environmental change, agriculture, geomorphology, archaeology, and other fields. However, these aerial surveys were unsystematic, not uniformly available across countries, and seldom used for tracking land cover changes over time (Kadmon and Harari-Kremer, 1999). Despite these challenges, when used properly, aerial images provide crucial historical insights about the Earth's surface and are vital for long-term studies.

In the past, image interpretation of B&W aerial photographs was a time-consuming and costly manual process (Wulder, 1998). To improve efficiency, experts need robust, repeatable, and inexpensive methods to mine these valuable data. Historical B&W aerial photographs, rich in spatial and radiometric (tonal) detail, are ideal for mapping fine-scale landscape features but demand extensive processing, storage, and computational resources. Google Earth Engine (GEE) has alleviated many problems related to large data management, storage, and processing (Boothroyd et al., 2021; Frake et al., 2020; Hansen et al., 2013; Joshi et al., 2016) and in doing so, has facilitated analyzing and mapping land-use and land-cover (LULC) changes across the globe (Kayitesi et al., 2022; Laurance et al., 2014; Pacheco Quevedo et al., 2023; Verburg et al., 2011; Yang et al., 2003).

In ordinary LULC analysis, classifications are based on the spectral signatures of different land cover types, however, due to the panchromatic nature of aerial B&W imagery, traditional pixel-based image analyses methods are limited. Object-based Image Analysis (OBIA), also called Geographic Object-Based Image Analysis (GEOBIA) (Hay and Castilla, 2008), has become popular for LULC classifications due to its ability to segment and classify landscape objects (henceforth referred to as "objects"). Furthermore, OBIA groups pixels together into objects to avoid the so-called 'salt and pepper' effect of more traditional pixel-based classifications (Blaschke, 2010; Vogels et al., 2017; Whiteside et al., 2020). OBIA builds on older methods such as segmentation, edge detection, feature extraction, and classification concepts with roots in industrial and medical image processing (Blaschke, 2010; Haralick et al., 1973). These methodologies are also still at the center of studies in the medical imaging field (Priyanka, 2020; Yang et al., 2012) as OBIA can produce high-quality results on high spatial resolution images.

Although most OBIA studies focus on the conversion of natural or agricultural areas to urban or exurban developments (Sealey et al., 2018; Tassi and Vizzari, 2020; Vogels et al., 2017), some studies have used the method to monitor landscape change in natural areas over time (Morgan and Gergel, 2010; Vogels et al., 2017). Others haves specifically shown how this approach has worked successfully in savanna type landscapes (Levick and Rogers, 2011; Whiteside et al., 2011, 2020). In dryland savannas, woody cover maps help describe the ecosystem's current state (Shafeian et al., 2021). Areas with high woody cover often indicate unfavorable shrub encroachment, which can reduce biodiversity and cause habitat fragmentation (Yang and Crews, 2019).

Kruger National Park (KNP) in South Africa, established in 1927, is one of the world's most expansive savanna protected areas. Aerial surveys, initiated in the late 1930s and conducted every 2 to 4 years since 2008, have covered KNP and other parts of South Africa. Although, previous studies have used the aerial surveys to reconstruct past landscapes of KNP, they were mostly limited to small and scattered areas. Eckhardt et al. (2000) used B&W aerial images of KNP from 1940 and estimated the woody cover in 20 sample plots of approximately 1.2 ha within nine transects of 75 ha primarily situated between the Sabie River in the south and the Olifants River in the north. Levick and Rogers (2011) focused only on the Shingwedzi catchment in the northern part of KNP. Munyati and Sinthumule (2016) mapped the woody cover using aerial images from 1940/1942 in four study sites across KNP (approx. 20,000 ha in total). For further information on the study sites used by Munyati and Sinthumule (2016) see Smit et al. (2013a).

In this study, we created a composite of high spatial resolution (0.5–0.75 m) B&W aerial images from 1939–1944 covering about 1.7 million ha of KNP. We then established a supervised learning workflow in GEE using an OBIA methodology with a Random Forest to classify the woody cover of the B&W composite of images. This large-area historical map offers the first comprehensive view of what the park's woody distribution (tall trees and shrubs) was like about 80 years ago, which until now was only partially understood through fragmented descriptions in period literature and small-area case studies.

This study will investigate and evaluate: (1) the extraction of information about woody vegetation from historical B&W high spatial resolution aerial images using a supervised learning workflow with an OBIA approach and (2) the implementation of the OBIA approach to classify the woody vegetation of large-area, high spatial resolution B&W aerial images. To contribute to understanding spatial distribution of woody cover historically, we present our results according to underlying geological substrates following previous studies that have highlighted their extreme importance in influencing the distribution of the woody cover in KNP (Eckhardt et al., 2000; Munyati and Sinthumule, 2016; Smit et al., 2013b; Urban et al., 2020).

2. Materials and methods

2.1. Study area

KNP is located in the northernmost part of South Africa, bordering Mozambique in the east and Zimbabwe in the north (Fig. 1). The climate varies between hot, humid summers (December–March) and mild, dry winters (June–August), with average maximum wet season temperatures around 34 °C and maximum dry season temperatures of 27 °C (Zambatis, 2003). This region receives the majority of its precipitation in the summer months, with a decreasing mean annual rainfall pattern seen from south to north and west to east (Gertenbach, 1980). The more arid bushveld north of the Olifants River (Fig. 1) receives 300–500 mm of rainfall annually, while the southern lowveld bushveld receives 500–700 mm annually (MacFadyen et al., 2018). KNP is divided from north to south by a lithological discontinuity (Fig. 1), with basalt rock underlying the eastern side and granitic rocks in the west. Soils that derive from granitic formation are considered nutrient-poor compared to the nutrient-rich basalt-derived soils.

The park is classified as a deciduous savanna and is characterized by the co-dominance of grasses, predominantly C_4, and an overstory of woody plants, which ranges from riparian forests to more open shrubs (Scholes and Walker, 1993). The south-west granitic part of KNP is characterized by mixed broadleaf woodlands dominated by important tree species such as red bushwillow (*Combretum apiculatum*), marula (*Sclerocarya birrea*), and knob thorn (*Senegalia nigrescens*), and by small-leaved shrubveld with thorny woody plants, such as sickle bush (*Dichrostachys cinerea)*. In the southeast, on basalt substrates, tree species include knobthorn, leadwood (*Combretum imberbe*) and marula.

Moving up, the granitic areas south of the Timbavati River (Fig. 1) are dominated by *Combretum* species and silver cluster-leaf (*Terminalia sericea*), while the granitic areas north of the river are covered by woodlands of mopane (*Colophospermum mopane*) and red bushwillow. The basalt areas between the Olifant and Sabie Rivers are dominated by savanna grasslands where the most common tree species are umbrella acacia (*Vachellia tortilis*), big marula trees, and the jackalberries (*Diosphyros mespiliformis*). The center-north areas of KNP, between the Olifants River and the Limpopo River, are the hottest and most arid and are dominated by medium-sized mopane trees.

There are also many riverine forests that follow the major perennial rivers (the Crocodile, Sabie, Olifants, Letaba, Luvuvhu, and Limpopo) (Fig. 1), which run from west to east. The riparian vegetation includes

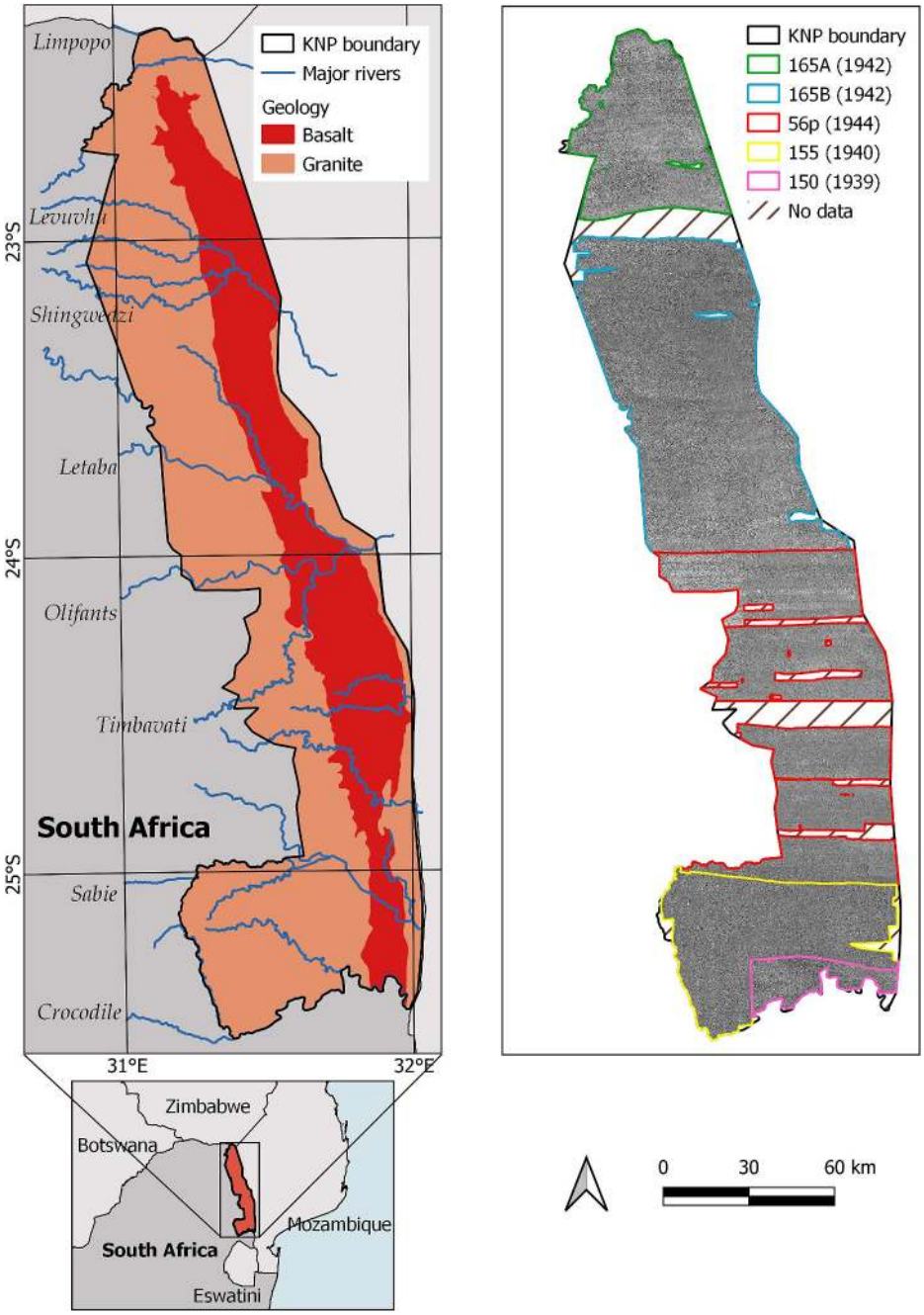

Fig. 1. On the left, the study area with a close-up of KNP highlighting the major rivers and the two main geological substrates, basalt, and granite. On the right, the full extent of the historical B&W aerial images used for the OBIA analysis together with the areas of No Data and the boundaries of the five photojobs with the corresponding color scale: 165A (1942), 165B (1942), 56p (1944), 155 (1940), and 150 (1939).

sycamore figs (*Ficus sycomorus*), nyala trees (*Xanthocercis zambesiaca)* and other riverine species. A detailed study on the vegetation of KNP was conducted by Gertenbach (1983) that classified KNP into 35 unique landscapes based on climate, soil, geomorphology, fauna, and vegetation studies. We later used these 35 landscapes to structure our sampling strategy.

2.2. Data collection

Using the first records of B&W panchromatic aerial photographs from 1939 to 1944 (KNP Scientific Services Data Repository), we generated a composite image mosaic of all B&W aerial images covering about 91% of KNP (Fig. 1). All images, comprising photojobs 165A, 165B, 56p, and 150 with a resolution of 0.5 m, and photojob 155 at 0.75 m (Table 1), were provided by the National Geospatial Information (NGI) of South Africa's Department of Rural Development and Land Reform. Selected from their flight plans to maximize KNP coverage, these historical photos were scanned at 1200 dpi into TIFF format without compression using an Epson Expression 10000XL A3 scanner with a transparency unit. The AAMgroup (now the Woolpert group-https://aamgroup.com) a private geospatial services consulting firm specializes in mapping and geospatial analysis, then orthorectified and combined each of these photojobs into an orthomosaic image.

The orthomosaic procedure performed by the AAMgroup comprised seven steps: (1) prepare the imagery (i.e., radiometric adjustments, such as contrast enhancements and intensity balancing, and image cropping

Table 1
Details of the five historical photojobs used to attain full coverage of KNP for the period 1939–1944.

Photojob	Scale	Format	Focal length	Resolution	Area (ha)
165A (1942)	1:30000	7"x7"	7"	0.50 m	238,727
165B (1942)	1:30000	7"x7"	7"	0.50 m	633,260
56p (1944)	1:20000	7"x7"	7"	0.50 m	513,781
155 (1940)	1:35000; 1:21000	7"x7"	4½"	0.75 m	277,629
150 (1939)	1:20000	7"x7"	7"	0.50 m	55,832

to fiducial marks to replicate digital frames in photogrammetry processing), (2) generate approximate photo center positions from flight plans, (3) import imagery into photogrammetry software and generate tie points using approximate photo center coordinates to line up photos, (4) measure control by scaling control points from new NGI imagery for plan and NGI DEM for heights, (5) perform aerial triangulation bundle adjustment solving for interior and exterior orientations, (6) run single frame orthos using NGI DEM and the mosaic, and (7) QA the resultant mosaic and fix errors.

2.3. OBIA workflow for woody cover classification

To test the methodology, we first focused on a subset of the aerial images and divided them into smaller subplots (approx. 25 km^2) (Fig. 2). Taking into account the diverse landscape of KNP we used Gertenbach (1983) vegetation map as a guide and labeled five subplots in the park's southern part based on the vegetation types (Fig. 2). The position of the subplots was guided by two factors: (1) geological substrate, in order to test the workflow based on the type of soil and (2) the presence of land cover elements, such as rivers or large rocks, in order to have a clear land cover element to test the accuracy of the segmentation process of the OBIA. Subplots 1–4 in photojob 155 are located on granite (Fig. 1), and subplot 5 in photojob 150 is located on basalt (Fig. 1). Quantum GIS (QGIS) 3.22 (QGIS Development Team, 2023) was used to clip the aerial photographs to the extent of the subplot boundaries.

To develop the supervised learning workflow to classify the woody cover from the B&W aerial images we used GEE and applied the OBIA methodology. The classification workflow to obtain the OBIA woody cover classification is divided into five steps: (1) data upload and script preparation (Section 2.3.1), (2) training/validation dataset (Section 2.3.2), (3) image segmentation (2.3.3), (4) woody cover classification (Section 2.3.4), and (5) accuracy, export, and land cover count (Section 2.3.5). An example of the GEE script is included in the Supplementary material.

2.3.1. Data upload and script preparation

To perform a land cover (LC) classification, GEE requires two initial inputs: an aerial image and the boundary of the area of interest. We uploaded the subplot boundary and the aerial images of each subplot as GEE assets. Once the assets were imported into our JavaScript-based program, the training/validation datasets could be created. Since we were interested in extracting the woody cover, we divided our training point features into two cover classes: 'non-woody' (LC property = 1) and 'woody' (LC property = 2). Woody cover was considered to be all vegetation with woody stems (i.e., excluding grasses and forbs), including trees that were shrubby (i.e., multi-stemmed) and short in

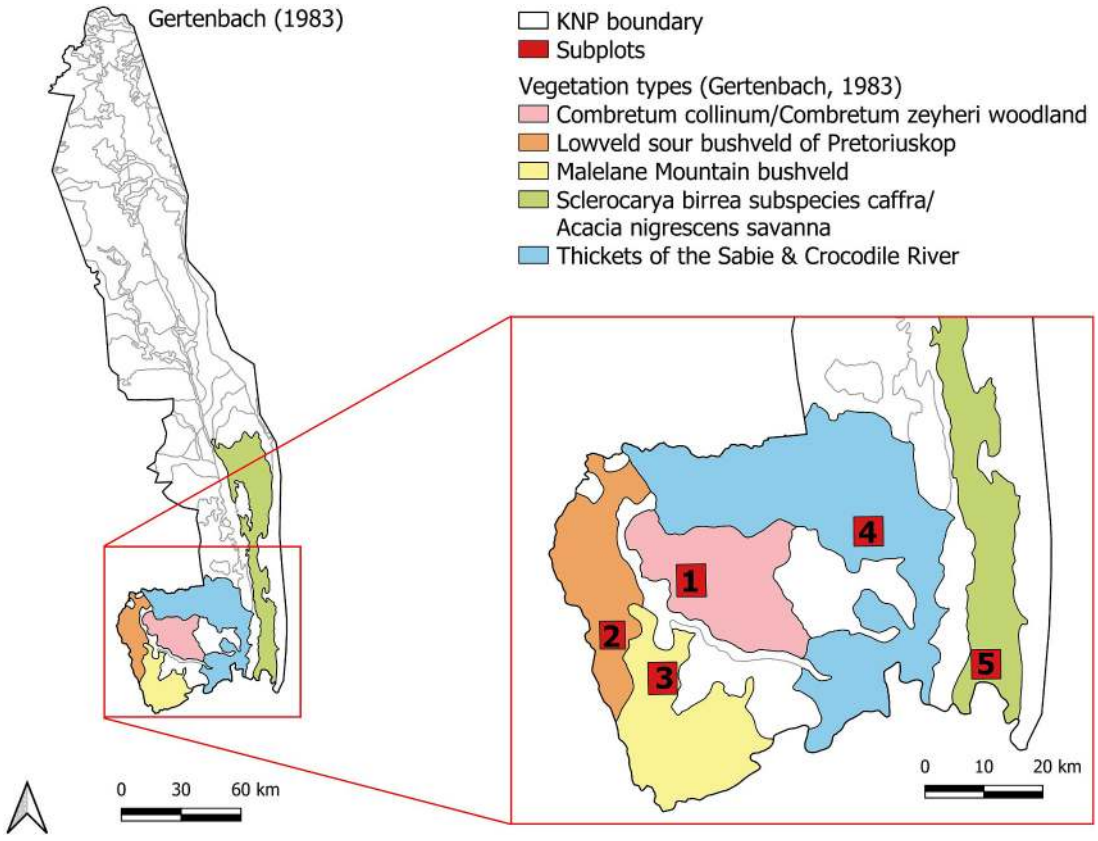

Fig. 2. On the left, we see the 35 vegetation types identified in Gertenbach (1983) in light gray in background with five vegetation types highlighted with different colors in the southern part of KNP. On the right, we show a zoom in image of the five highlighted vegetation types where we placed five subplots (approx. 25 km^2), in red, that were used to test the methodology further explained in Section 2.3. (For interpretation of the references to color in this figure legend, the reader is referred to the web version of this article.)

stature.

2.3.2. Training/validation dataset

Most studies dealing with data sampling recommend the use of random or stratified sampling approaches to generate training/validation points (Hammond and Verbyla, 1996; Millard and Richardson, 2015; Tassi et al., 2021). In this study, a set of 400 random points was generated within the subplot, and subsequently the points were assigned to one of the two LC classes. The number of random points was based on trial-and-error classifications that were run in the same areas. Random points that fell on a specific pixel were labeled by visual interpretation as either 'non-woody' or 'woody'. Important considerations while deciding the class of the pixel were (1) pattern of the pixels within which the random point fell, (2) shape of the object, and (3) grayness of the pixel.

However, in an open savanna environment like KNP, where the probability of a random point landing on a woody plant is exceptionally low, a completely random sampling protocol produced an unbalanced training set and resulted in the misclassification of smaller woody plants (i.e., shrubs). To address this issue, we created a separate geometry, 'add trees' (LC property = 2), whereby well-defined examples of woody cover elements were added until the two classes had the same number of training points. This new geometry was then merged with the randomly allocated woody points, 'woody' (LC property = 2) + 'add trees' (LC property = 2) = 'merged woody', as they are part of the same land cover class. To assess model accuracy, we then randomly separated 80/20% of the classified points to generate a training/validation dataset to be used later in the accuracy assessments.

2.3.3. Image segmentation

We used a bottom-up, seed-based segmentation algorithm in GEE called Simple Non-Iterative Clustering (SNIC) based on parameters of compactness, connectivity, and neighborhood size (Achanta and Susstrunk, 2017). The "compactness" influences the shape of the clusters (larger values produce more compact clusters), the "connectivity" defines how to merge adjacent clusters, and the "neighborhoodSize" avoids tile artifacts. The values of the SNIC parameters for this study are present in the GEE script included in the Supplementary material. For further description of the segmentation approach, we refer to the work of Achanta and Susstrunk (2017) and a recently published book on GEE (Cardille et al., 2024). We adopted the two-step procedure presented in Tassi and Vizzari (2020) that combines the SNIC segmentation algorithm with a Gray-Level Co-occurrence Matrix (GLCM). GLCM is a second-order statistical method for extracting textural metrics from gray-scale images and examines the spatial relationships between pixel intensities in an image to quantify texture, providing insights into patterns, and variability within the data.

The GLCM metrics describe the texture of an object, intended as the spatial arrangement of the brightness values within an object. In total, 18 GLCM texture metrics were derived for each object, 14 metrics proposed by Haralick et al. (1973) and an additional four metrics added by Conners et al. (1984). For the spatial clustering step of the classification, we used GEE's "Image.Segmentation.seedGrid" algorithm that works with superpixels, a concept first introduced by Ren and Malik (2003) and then further developed by Achanta and Susstrunk (2017) which groups pixels together to obtain a more natural and homogenous structure. For the purpose of this study, a superpixel seed location spacing of 15 was chosen as the grouping pixel size, considering the textural characteristics of the landscape patches.

2.3.4. Woody cover classification

To obtain the woody cover classification we chose the Random Forest classifier, which is a supervised learning algorithm that produces multiple decision trees using a randomly selected subset of training data and independent variables (Breiman, 2001). It has received much attention in the last few years due to its excellent classification results, fast-processing speed, ease in handling different types of data, e.g., shape and texture, and no requirement for normally distributed data (Belgiu and Drăguţ, 2016; Rodriguez-Galiano et al., 2012; Vogels et al., 2017). Another advantage of the Random Forest is that it is able to compute variable importance measures that allow us to identify the variables that exerted a substantial influence on the classification process (Rodriguez-Galiano et al., 2012).

For assessing the variable importance of the 18 GLCM texture metrics, we utilized the "ee.classifier.explain" algorithm and then calculated the relative importance of each metric. In contrast to other image classification software, the segmentation process is performed after the training dataset is created, therefore, the objects obtained from the SNIC algorithm (Section 2.3.3) are then labeled with the corresponding LC labels of the training points collected in Section 2.3.2 as preparation for image classification with the chosen classifier. Therefore, using the Random Forest together with the GLCM texture metrics (independent variables) and the training samples identified with LC labels (dependent variable), we classified all other segmented objects into woody or non-woody LC to obtain the final woody cover classification image.

2.3.5. Accuracy, export, and land cover count

After each aerial image was classified, we evaluated the accuracy metrics using a confusion matrix in GEE to summarize the performance of our classification workflow (Radoux et al., 2008). Factors that affected the measurement of accuracy included the resolution of the aerial images, the training/validation dataset, and the LC classes chosen. Accuracy assessment of the performance of the Random Forest classification yields values ranging from 0% (no match) to 100% (complete match) (Lillesand et al., 2004). Overall accuracy reflects the percentage of correctly classified pixels in a map, but it does not show how errors are distributed among different land cover classes. To address this, we calculated producer's accuracy, which gauges the correctness of reference pixel classification, and user's accuracy, which indicates how accurately the classification represents actual ground conditions. To overcome computational limits in GEE, we divided our output into smaller tiles and exported each OBIA woody cover classification subset to Google Drive for post-processing and analyses. To calculate the percentage of woody and non-woody land cover we used QGIS.

2.4. Large-area, high spatial resolution woody cover classification

After refining our supervised learning workflow for woody cover classification using OBIA on the five small subplots (Fig. 2), we faced two challenges in applying the methodology to the broader set of aerial photojobs (Table 1): first, working with a mosaic of images from different years and characteristics adds complexity; second, processing and handling large areas requires significant storage and computational resources. Moreover, a small part of the image from photojob 155 (1940) was omitted due to the diminished panchromatic fidelity and incidence of artifacts, indicative of the aerial photographs' degradation over time. The total area of the photojobs included in the OBIA classification is shown in Table A.1. To address both issues, we treated each photojob separately, divided the photojobs into smaller boundaries (Fig. A.1), and performed the OBIA woody cover classification on each.

The supervised learning workflow adheres to the steps outlined in Sections 2.3.1–2.3.5. However, as detailed in Section 2.3.2, we deviated by not generating 400 random points over the entire boundary. Instead, we used the vegetation types described by Gertenbach (1983) to guide the placement of our sampling plots, from which we then collected the training and validation points (Fig. A.2). The creation of several small sampling plots within each vegetation type, instead of using one large area, also helped speed up the sampling process. Performing the data collection within the sampling plots ensured that we had training/validation points that were representative of the diverse vegetation within each boundary. To determine the size of the sampling plots, we first calculated 5% of the total area covered by the boundary, divided that area by the number of vegetation types intersecting the boundary

and then proceeded to label the sampling plots based on vegetation type. However, if a vegetation type was too small to accommodate the entire sampling plot, we placed the largest area within that vegetation type, while assigning the remaining area to the nearest largest vegetation type.

The position of the sampling plots was chosen based on (1) quality of the historical image, (2) recognizable objects (rivers, large rocks, roads), and (3) distance to other sampling areas. Once we labeled the sampling plots based on vegetation type, we generated 400 random points across the sampling plots. After collecting the training/validation points, as seen in Section 2.3.2, we followed the steps in Section 2.3.3–2.3.5 to obtain the OBIA woody cover classification and accuracy measurements of each individual photojob boundary. The final OBIA classification results are presented for each photojob. An example of the methodology is shown in Fig. A.2, in which the five sampling plots (a - e) are located inside the five vegetation types (Gertenbach, 1983) intersecting one of the individual boundaries of photojob 56p (1944).

3. Results

The resulting woody cover classification of the five subplots (Fig. 2) had a high overall accuracy in all subplots (Table 2). Subplot 5 on basalt soils had the lowest overall accuracy (84%) with a producer's accuracy value for the woody cover class of 76%, indicating a higher probability of misclassification. Subplot 1 on the granitic soils had the highest percentage of woody cover (25%) while the lowest percentage (10%) was recorded on the basalt soils on subplot 5. The highest value of overall accuracy obtained was 95% in subplot 3. The producer's and user's accuracy for subplots 1, 2, 3, and 4 indicate low errors of commission and omission, suggesting a low probability of misclassification on granite. In Fig. 3, we present an enlarged extract of the OBIA woody cover classification for each of the five subplots.

When performing the OBIA on all photojobs, the overall accuracies remained high, with photojob 165A (1942) in the north having the highest values for overall accuracy (92%) (Table 3). Similarly, the producer's and user's accuracy parameters indicate low errors of commission and omission (Table 3) and thus low probability of misclassification for all photojobs. Photojob 165A (1942), 155 (1940), and 150 (1939) had the lowest percentages of woody cover, 19%, 23%, and 22%, respectively, while the central areas of KNP, covered by photojobs 165B (1942) and 56p (1944) had the highest values, 29% and 28% respectively (Table 3). Furthermore, we also calculated the total percentage of non-woody cover (74%) and woody cover (26%) of the composite of photojobs, with an overall accuracy of 89%, producer's accuracy (non-woody = 88%, woody = 90%), and user's accuracy (non-woody = 90%, woody = 87%). In Fig. 4, we present an enlarged extract of the OBIA woody cover classification for each of the five photojobs. Supplementary material includes a link to a full image of the woody cover classification of KNP in an A0 format (Fig. S.1) and all individual OBIA woody cover classifications for each individual photojob can be downloaded freely.

Table 2
Statistics for each Subplot include percentage of Non-woody (NW) and Woody (W) cover (%), Overall accuracy, Producer's accuracy (%), and User's accuracy (%).

Subplots	Non-woody cover (%)	Woody cover (%)	Overall accuracy (%)	Class	Producer's accuracy (%)	User's accuracy (%)
1	75	25	86	NW	84	88
				W	87	83
2	87	13	93	NW	96	91
				W	91	96
3	86	14	95	NW	98	91
				W	92	98
4	81	19	89	NW	89	90
				W	90	88
5	90	10	84	NW	92	80
				W	76	90

The analysis of the woody and non-woody cover and geological substrate showed that, on average, the percentage of woody cover is lower on basalt than on granite (Table 4). Photojob 165A had the lowest percentage of woody cover on basalt (11%), while granite had more than double the percentage of woody cover (23%). We also calculated the percentage of woody and non-woody cover in the composite images for each geological substrate. In basalt areas, the total woody and non-woody cover was 21% and 79%, respectively. Granite, averaged across vegetation types, had a higher percentage of woody cover (28%) and a lower percentage of non-woody cover (72%) than basalt.

Analyzing the variable importance for each OBIA classification for both the subplots (Fig. A. 3) and the photojobs showed comparable results (Fig. A.4). However, as the OBIA classifications per photojob were run on smaller boundaries, to better highlight the variance between the different classifications we used a boxplot to show the importance of each GLCM texture metric, highlighting the minimum and maximum value (Fig. A.4). The four most important GLCM texture metrics are: mean-difference-to-neighboring brightness, sum average, cluster shade, and correlation.

4. Discussion

The historical aerial images covering KNP provided an opportunity to apply OBIA to a large dataset (approx. 1.7 million ha) and to create a methodology tailored to classify land cover of B&W historical photographs. This methodology was an iterative process built on previous studies in the field (Eckhardt et al., 2000; Fensham and Fairfax, 2002; Hay and Castilla, 2008; Tassi and Vizzari, 2020; Vogels et al., 2017) and on new site-specific methods. We first developed a supervised learning workflow in GEE that detects woody cover from B&W images and then conceptualized an efficient training/validation sampling strategy that was applied to create the first historical woody cover map of KNP in 1939–1944.

The accuracy of land cover classification through OBIA differed across various landscapes. This variance is attributed to the diverse characteristics of natural features like trees and shrubs, including their size, shape, and height (Drăguţ et al., 2009; Tassi and Vizzari, 2020; Vogels et al., 2017). Consequently, selecting appropriate parameters for the OBIA segmentation process was crucial for achieving accurate classifications. The variable importance analysis of each GLCM texture metric on both the subplots (A.3) and the photojobs (A.4) highlighted how the most important variables are the same, indicating a consistency overall in the analysis, independent of the photojob and the geological substrate.

In the past, most studies that adopted GLCM texture metrics for land cover assessments were focused on agricultural areas (Abu et al., 2021; Vogels et al., 2017). Vogels et al. (2017) assessed land degradation with a semi-automated methodology to map cropland using B&W photographs and found that the most important GLCM texture metrics were homogeneity, angular second momentum, and entropy. However, the variables most important for identifying small natural elements, such as woody vegetation differ compared to man-made objects such as agricultural fields. A recent study by Park and Guldmann (2020) that analyzed the correlation between the GLCM texture metrics and commonly used landscape metrics to study landscape fragmentation shows that the GLCM mean-difference-to-neighboring brightness texture metric is highly correlated with the PLAND landscape metric (i.e., percentage of tree patches in a landscape) and that the GLCM correlation texture metric appears to be strongly associated with the level of patch aggregation in an image. These results confirm the importance of including GLCM texture metrics as attributes to help classify and distinguish woody cover elements in the landscape.

Moreover, in the medical field, the GLCM cluster shade texture metric is widely used to highlight the degree of skewness (i.e., when the

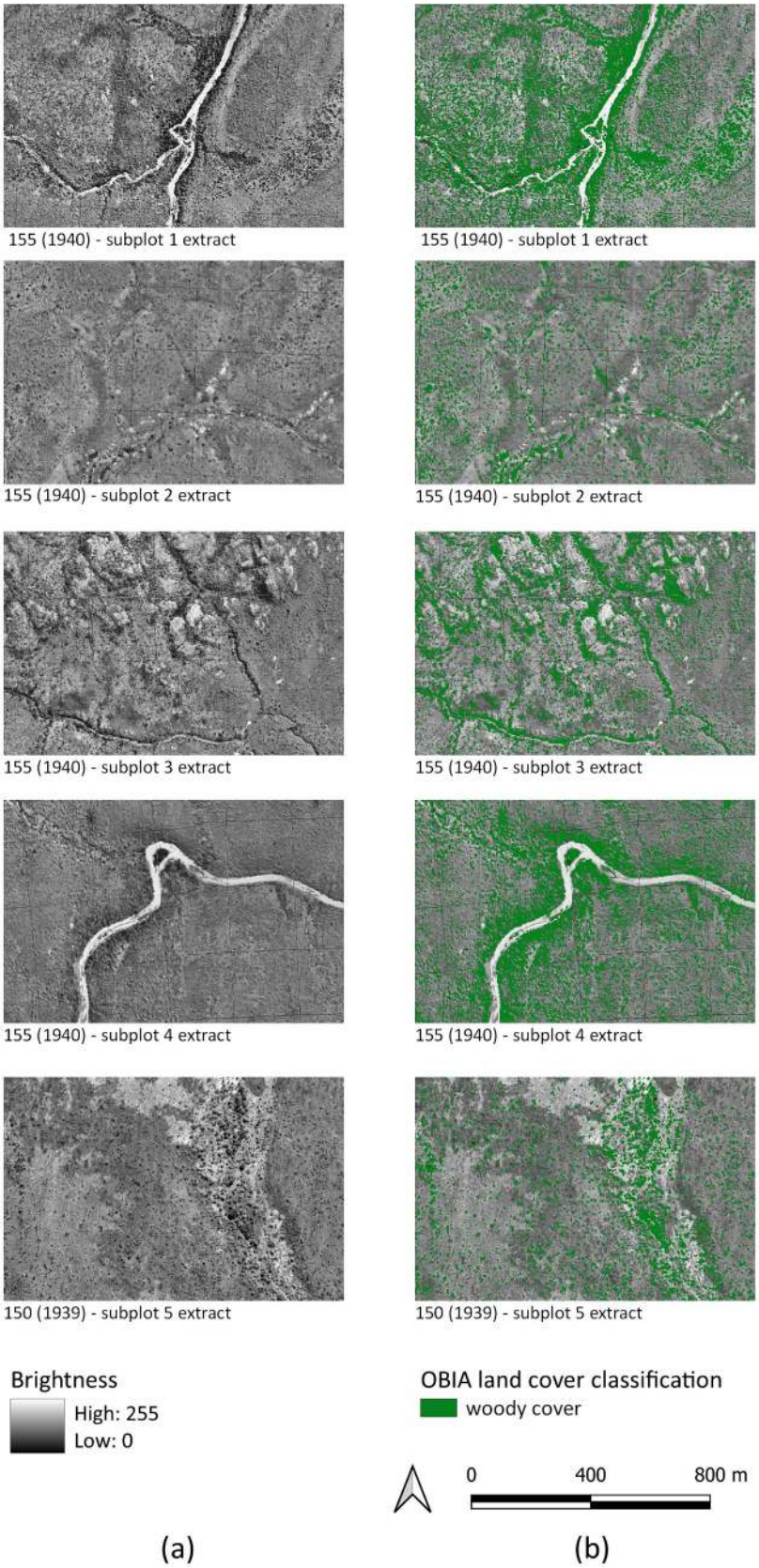

Fig. 3. a) Extracts of the original B&W aerial image of the five subplots described in Fig. 2; b) Results of the OBIA classification of the woody cover of the aerial images in a).

Table 3
Statistics include percentage of Non-woody (NW) and Woody (W) cover (%), Overall accuracy, Producer's accuracy (%), and User's accuracy (%) per photojob.

Photojob	Non-woody cover (%)	Woody cover (%)	Overall accuracy (%)	Class	Producer's accuracy (%)	User's accuracy (%)
165A (1942)	81	19	92	NW	91	92
				W	92	91
165B (1942)	71	29	87	NW	85	90
				W	89	83
56p (1944)	72	28	89	NW	90	89
				W	88	90
155 (1940)	77	23	91	NW	88	92
				W	94	91
150 (1939)	78	22	83	NW	85	85
				W	81	81

cluster shade is high the image is asymmetric). A recent study by Abu et al. (2021), focused on the fragmentation of cocoa farms in Côte d'Ivoire and Ghana, identified the cluster shade as the most significant GLCM texture metric for the Random Forest classifier. Therefore, considering our findings and existing research in the field, we propose that GLCM texture metrics such as mean-difference-to-neighboring brightness, sum average, cluster shade, and correlation play a significant role in comprehending landscape composition, symmetry, and aggregation (Figs. A.3 and A.4).

The analysis performed at the subplot level helped us define the segmentation parameters, fine tune the training/test sampling strategy, and finalize the classification process. The classification of woody cover performed better on granite than on basalt soils (Table 2), which could be due to the darker background color of the basalt soils and overall lower percentage of woody cover on basalts, as confirmed by more recent studies in KNP (Munyati and Sinthumule, 2016; Urban et al., 2020). Roads, rivers, and rocks contrasted sharply in shape and color with the vegetation and, as a result, were accurately classified (see extracts of subplots 1, 3 and 4 in Fig. 3b) as opposed to small trees on dark soils (extract of subplot 5 in Fig. 3b). Furthermore, subplot 5 had a low producer's accuracy value for the woody cover class (76%) (Table 2), indicating that the woody land cover class could have been overestimated in relation to the reference data.

Our findings that subplots 1 and 4 (Fig. 2), on granite, had the highest woody cover, 25% and 19%, respectively (Table 2), align with the overall results of Eckhardt et al. (2000), which found a mean cover of 20% on granites in the 1940's aerial images of KNP. Subplot 5 (Fig. 2) located on the basalt areas near Lower Sabie had the lowest woody cover (10%), a result also confirmed by Eckhardt et al. (2000) which calculated a mean of 12% woody cover on basalts for the 1940s. On the other hand, subplots 2 and 3 (Fig. 2) had a lower woody cover, 13% and 14%, respectively, even though they are also on granitic soil. However, it is important to recognize that Eckhardt et al. (2000) focused their study on the southern-central part of KNP, using aerial photographs from 1940, 1974, and 1998, as well as fixed-point photographs from 1984 and 1996. They employed IDRISI software to segment and classify these images, identifying distinct objects or areas such as woody vegetation and categorizing them based on their spectral and spatial properties to estimate woody cover. Due to the specific location and unique methodology of their study, direct comparisons with our results may not be feasible.

Based on historic photographs and the diaries of Stevenson-Hamilton, first published in 1937 (Stevenson-Hamilton, 1993), the areas around subplot 2 (Fig. 2) in the lowveld sour bushveld of Pretoriuskop and subplot 3 (Fig. 2) in the Malelane mountains, were highly grazed, especially by livestock, with frequent early season burns (Wolhuter, 2010), which may explain why the woody cover was lower in these subplots. Therefore, with regard to previous studies and the results obtained in the subplots, the difference in woody cover across the park could be attributed to the dynamics of the vegetation in relation to soil properties (Knoop and Walker, 1985) which, in turn, interact with productivity and disturbances such as herbivory and fire (Du Toit et al., 2003).

The results performed at the photojob level (Table 3) are comparable with the previous analyses performed for the subplots (Table 2). Photojob 165A (1942) in the north and photojobs 155 (1940) and 150 (1939) in the south had a lower percentage of woody cover than the central areas of the park 165B (1942) and 56p (1944) (Table 3). The woody cover in photojob 155 (1940) may be slightly overestimated due to the presence of artifacts (i.e., dark green spots shown in Fig. S.1) misclassified as woody vegetation. However, the OBIA classification results for photojob 155 (1940) are comparable to the adjacent photojob 150 (1939), which suggests that overestimation may not be a problem. The woody cover classification of the five photojobs represents the first large-area, high spatial resolution historical analyses of woody vegetation across KNP.

To better understand the spatial distribution of vegetation, we followed previous studies that have highlighted the importance of geological substrates in KNP (Eckhardt et al., 2000; Munyati and Sinthumule, 2016; Smit et al., 2013b; Urban et al., 2020) and calculated the percentage of woody cover on basalt and granite separately (Table 4). Overall, the percentage of woody cover on basalts is 21% while it is higher on granites, at 28%, a difference clearly visible in Fig. S.1. These results support the broader understanding of vegetation distribution within KNP's savanna ecosystems as outlined by Du Toit et al. (2003). Granitic, sandy soils, with less palatable vegetation for herbivores, lower intensity fires, and lower competition, have more dense savannas with a higher number and cover of woody plants, while basaltic, clay soils support higher grass biomass, resulting in more intense fires and more open landscapes.

The lowest percentage of woody cover on basalt soils (11%) was obtained in photojob 165A in the northernmost part of KNP, while the highest percentage on basalt, 23%, was recorded in the central part of KNP for both photojob 165B and 56p (Table 4). This result could be explained by a more semi-arid environment in the north as opposed to a subhumid climate in the south (Trabucco and Zomer, 2014). The percentage of woody cover on basalts obtained for photojob 155 (1940), 19%, could be slightly lower due to the artifacts in the aerial image (Fig. S.1), yet they are comparable with the results for photojob 150 (1939) (Table 4). The highest percentages on granite soils were recorded in the central areas of KNP (photojob 165B and 56p), approximately 30%. The higher woody cover on both granite and basalt in the central areas could be attributed to the mopane trees (*Colophospermum mopane*) that dominate these hot and dry environments.

We obtained higher values of woody cover for photojob 56p, 23% for basalts and 30% on granites, than what Eckhardt et al. (2000) presented in their study (on average 12% for basalts and 20% for granites). These higher results could be attributed to the differences in methodologies adopted, specifically, the different sizes of the sampling area and the divergent dates of the aerial images. Eckhardt et al. (2000) used an area of approximately 200 ha over 9 transects as opposed to approximately 500,000 ha covered by photojob 56p and used aerial images from 1940 as opposed to those from 1944 in photojob 56p. However, overall, the woody cover was higher on granites than on basalts as confirmed by Eckhardt et al. (2000) and this study, and the difference in percentage

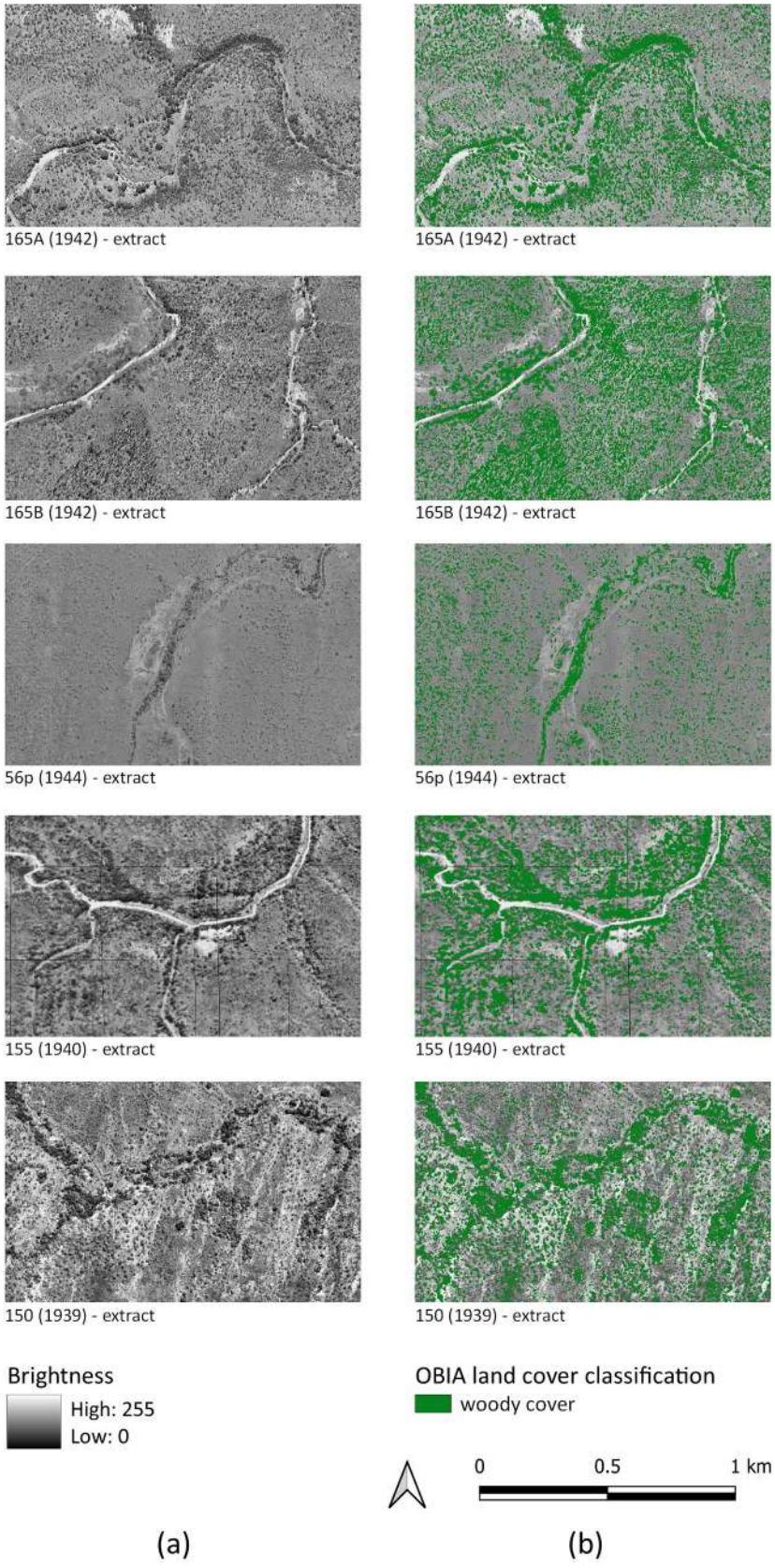

Fig. 4. a) Extracts of the original B&W aerial image divided per photojob described in Fig. 1; b) Results of the OBIA classification of the woody cover of the aerial images in a).

Table 4
Non-woody (%) and Woody cover (%) of each photojob per geological substrate.

Photojob	Class	Non-woody cover (%)	Woody cover (%)
165A (1942)	Basalt	89	11
	Granite	77	23
165B (1942)	Basalt	77	23
	Granite	68	32
56p (1944)	Basalt	77	23
	Granite	70	30
155 (1940)	Basalt	81	19
	Granite	77	23
150 (1939)	Basalt	84	16
	Granite	78	22

between geological substrates is approximately at 8% for Eckhardt et al. (2000) and 7% for photojob 56p.

Previous studies in KNP have shown that the combination of abiotic factors like rainfall, geological substrate, soils, fire regimes, and biotic factors like herbivores have created the park's complex environmental mosaic we see today (Du Toit et al., 2003; Scholtz et al., 2014; Smit et al., 2010; Urban et al., 2020). Eckhardt et al. (2000) and Munyati and Sinthumule (2016) performed a land cover change analysis to better understand vegetation dynamics linked to the geological substrate in KNP, yet both studies considered small or scattered study sites (approx. 200 ha over 9 transects and 4 sites of approx. 20,000 ha in total, respectively).

Large-area studies are necessary to fully understand the dynamics linked to the main drivers of vegetation change in savannas and more specifically in KNP. Urban et al. (2020) mapped the woody cover of KNP using Sentinel-1 (10 m spatial resolution) for the years 2016–2017. They found that the highest woody cover percentages were reached in the northern part of KNP on sandy granite-derived soils, while the lowest values were found on the basalt areas in the eastern part of KNP, highlighting how the woody cover in KNP is significantly controlled by the underlying geological substrate and the north-to-south rainfall gradient. The results of this study could be used for land cover change analysis as a historical baseline to document how the woody cover has changed through time in KNP, even though for comparative studies using images at the same spatial scale would be advisable.

Moreover, the results of this study provide a snapshot of what the park looked like with low densities of herbivores in the landscape and with no active fire management strategies implemented. In 1946 Stevenson Hamilton in the *Kruger National Park, warden's annual report* counted only 400–450 elephants in the entire park (Stevenson-Hamilton, 1993), as opposed to 17,086 counted in 2015 (Ferreira et al., 2017). In the light of concerns around accelerated elephant impacts in KNP (Das et al., 2022), the results of this study could be used to help formulate future elephant management strategies.

As with any other type of remotely sensed data and image analysis approach, there are challenges in this study that need to be taken into consideration with the interpretation of the results. The biggest challenge was working with a mosaic of historical B&W aerial images from different years together with compiling the training/validation dataset for large-area, high spatial resolution aerial images. Therefore, it was essential to build an easy and efficient sampling strategy and export methodology. GEE played a significant role in this process, as it allowed different independent operators to collect training and test samples using a cloud-based server to run the analyses which minimized large data management and storage. Furthermore, as mentioned in Section 2.4, photojob 155 (1940) was the aerial image with the highest number of visible artifacts (i.e., dark round green circles) and this can be observed looking at this area in Fig. S.1. For this reason, a part of this photojob was eliminated from our analysis (Table A.1) as the quality and presence of artifacts highly compromised our classification. Other artifacts due to image quality (i.e., horizontal lines) are present in photojob 56p (Fig. S.1), however, the overall distribution of the woody cover is consistent and overall accuracy, the producer's accuracy, and consumer's accuracy are all high, validating the result.

The presence of shadows around trees has also been mentioned as an issue surrounding woody cover classification of B&W images (Fensham and Fairfax, 2002). Manual techniques applied for the training/validation dataset have been shown to represent a major advantage to avoid shadow effects (Fensham et al., 2002) and the balance of the producer's accuracy and the consumer's accuracy obtained in our analyses for all photojobs indicates a low misclassification error. This historical study focuses on woody cover, defined as both trees and shrubs. A future stereoscope analysis could help better understand the ongoing process of the encroachment of small trees and shrubs in African savannas (Coetsee et al., 2023). Lastly, another challenge for panchromatic images is fire scars, often widespread in African savannas. In this study, it was not necessary to exclude burned areas from the analysis because few of these were present. It would be advisable for further studies of B&W photographs that show extensive burned areas to exclude them from the classification to avoid woody cover overestimation.

5. Conclusions

The analysis of B&W images is clearly challenging; nonetheless, it represents an essential piece of the puzzle for long-term LULC analysis. Historical datasets provide valuable insights into past landscapes, enhance conservation efforts, and support evidence-based decision-making. This study represents the first historical woody cover baseline for KNP dating back 80 years and covering an extent of about 1.7 million ha with important implications for assessing the impact of past human activities, gauging the effectiveness of implemented management strategies, and setting future conservation priorities.

Leveraging freely available satellite imagery and cloud-based computing platforms like GEE, conservationists can analyze large-area, high spatial resolution land cover changes and, based on that make informed decisions regarding habitat restoration, invasive species management, and fire regimes. Therefore, the implications of this research extend beyond KNP because the developed methodology can be replicated in other ecosystems and protected areas and contribute to landscape management and environmental planning.

The results obtained in this study can be used as a baseline for future LULC analysis performed with other methodologies, such as deep learning CNN (Jagannathan and Divya, 2021). Going forward, the analysis of aerial images of KNP taken about every two years deep learning methods will be most effective and useful to map land cover or more specifically woody cover. Integrating large-area historical datasets in land-use and land-cover analysis can serve as a resource to better understanding long-term landscape changes and support ecological monitoring programs. The results of studies such as this one can be used to better protect and preserve our natural heritage, enable effective management strategies, and contribute to the conservation of global biodiversity.

CRediT authorship contribution statement

Tullia Riccardi: Conceptualization, Methodology, Software, Validation, Visualization, Writing – original draft, Writing – review & editing. **Benjamin J. Wigley:** Conceptualization, Methodology, Software, Validation, Writing – review & editing. **Linda Kleyn:** Conceptualization, Methodology, Software, Validation, Writing – review & editing. **Corli Coetsee:** Conceptualization, Methodology, Writing – review & editing. **Sandra MacFadyen:** Conceptualization, Methodology, Software, Writing – review & editing. **Fabio Attorre:** Conceptualization, Writing – review & editing. **Luca Malatesta:** Conceptualization, Methodology, Software, Supervision, Writing – review & editing.

Declaration of competing interest

The authors declare no conflict of interest.

Data availability

We have shared the data in a link within the Supplementary material

Acknowledgements

We thank the anonymous reviewers for their constructive comments and suggestions that greatly improved the quality of the manuscript. We acknowledge the financial support of the Italian Agency for Development Cooperation AICS through the COREBIOM – Conservation and Renovation for Biodiversity in Mozambique (AID 12042) and of the National Research Foundation: South Africa (Grant 89967). Thank you to the AAMgroup (now the Woolpert group) for digitizing and georeferencing the aerial images. We thank Michelle Denner and Amanda Pypers from the National Geo-spatial Information (NGI) in Mowbray for their continued support and help with collating and scanning the historical aerial imagery. We also thank Camilla Foggia, Chiara Benvenuti, Francesca Romana Trezza, Francesco Narduzzi, Francesco Segatori, Mathieu Sgriccia, Martina Osimani, Marzia Magro, Serena Baini, Valentino Mundo, Violetta Parutto, and Virginia Cuccaro for helping with the data collection and validation.

Appendix A. Appendix

Table A.1
Total area in hectares (ha) covered by the B&W aerial images during the OBIA classification.

Photojob	Area (ha) for the OBIA
165A (1942)	238,727
165B (1942)	633,260
56p (1944)	513,781
155 (1940)	262,052
150 (1939)	55,832
Total	**1,647,820**

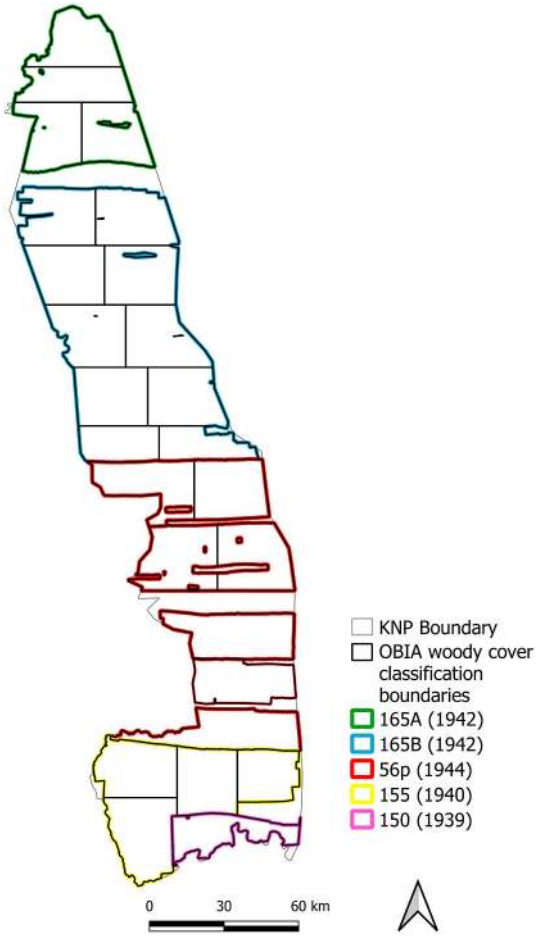

Fig. A.1. The outline of the boundaries that are used to perform the individual OBIA woody cover classification. We highlight the boundaries of each photojob with the corresponding color scale.

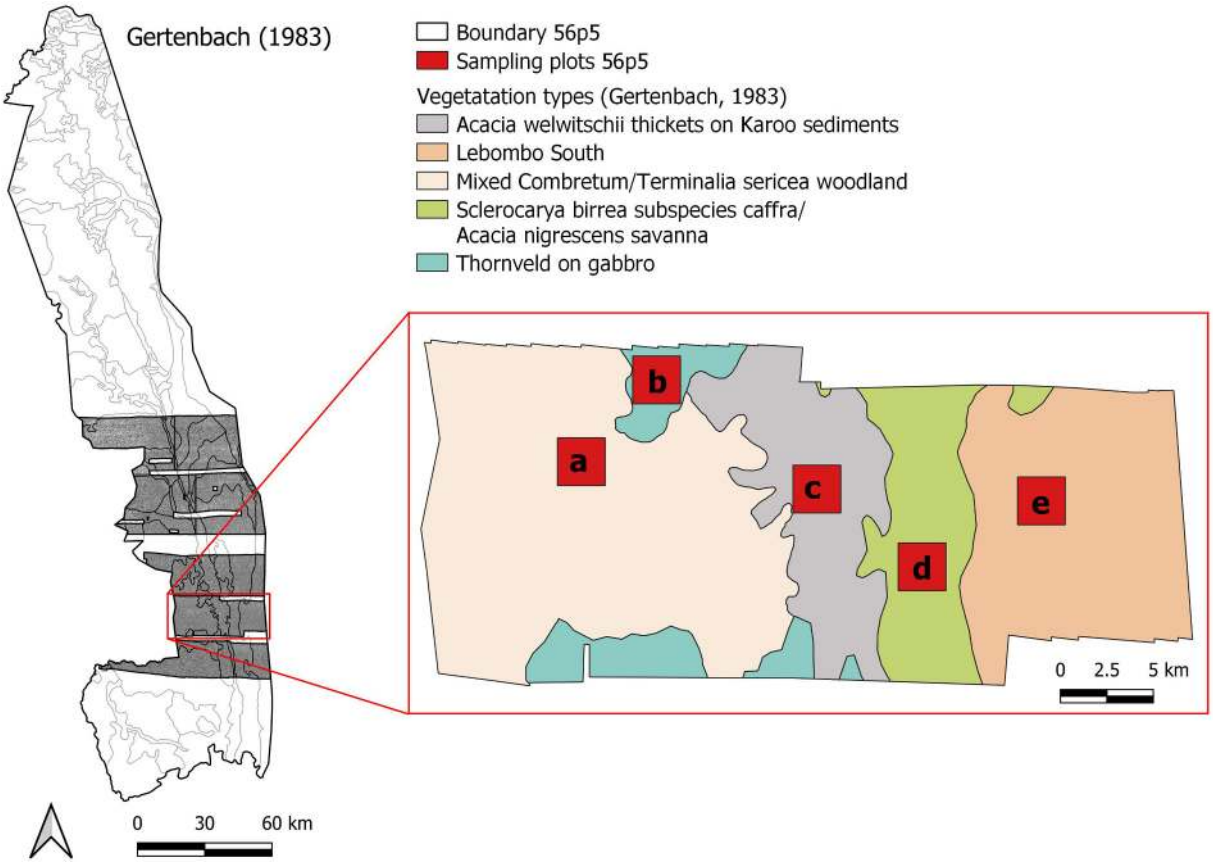

Fig. A.2. On the left, the 35 vegetation types identified in Gertenbach (1983) are shown in light gray in the background together and the seven separate boundaries of photojob 56p (1944) used to perform the OBIA classification (Fig. A.1) with the original B&W aerial images; On the right, we see a close up of the sampling methodology for boundary 56p5, with the sampling areas in red placed within the five vegetation types that intersect the boundary. (For interpretation of the references to color in this figure legend, the reader is referred to the web version of this article.)

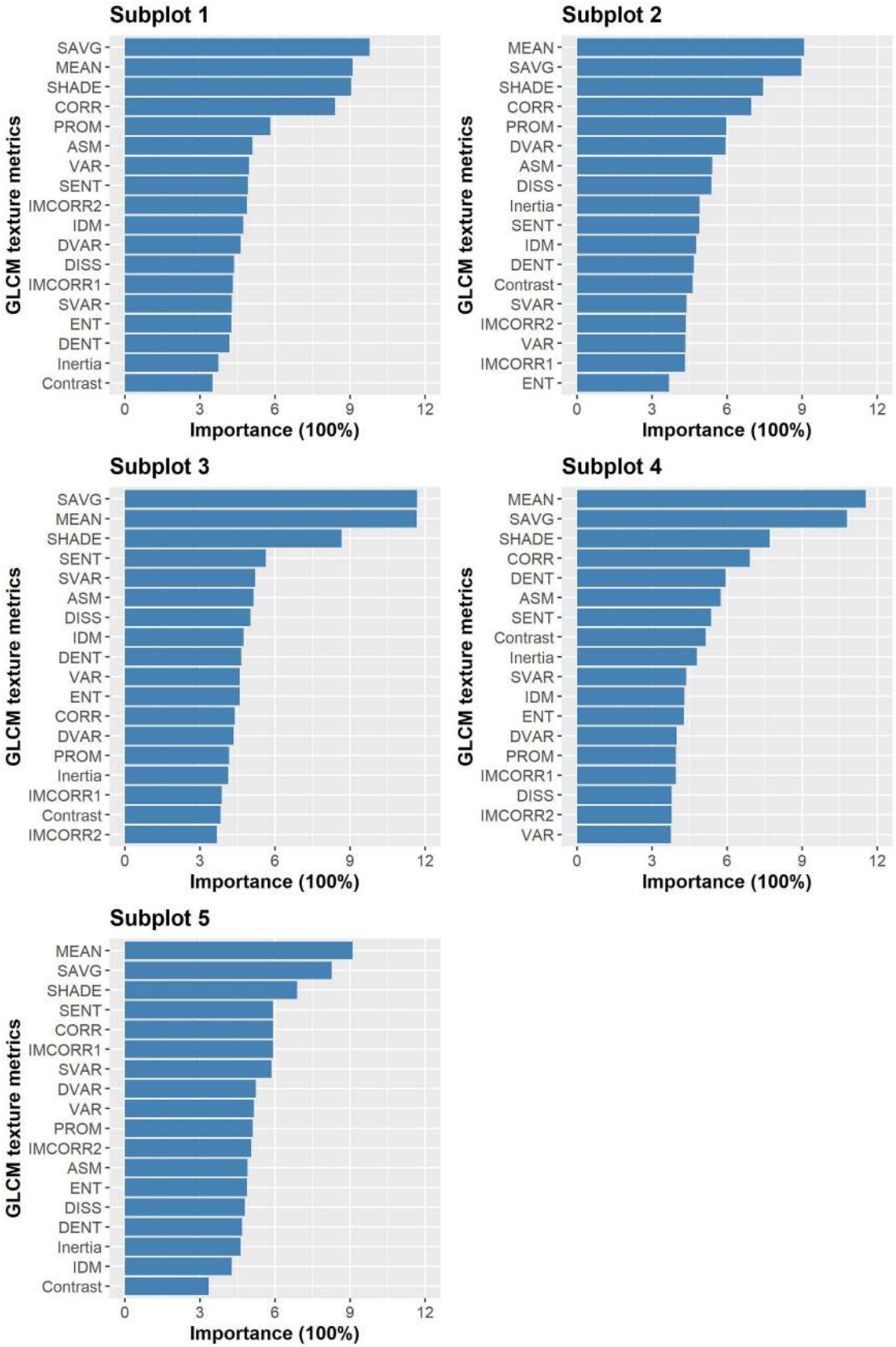

Fig. A.3. Variable importance of GLCM texture features for each subplot 1–5 (Fig. A.1). The GLCM features: ASM = angular second moment, Contrast, CORR = correlation, DENT = difference entropy, DISS = dissimilarity, DVAR = difference variance, ENT = Entropy, IDM = inverse difference moment, IMCORR1 = information measure of Corr. 1, IMCORR2 = information measure of Corr. 2, Inertia, MEAN = mean-difference-to-neighboring brightness, PROM = cluster prominence, SAVG = Sum Average, SENT = sum entropy, SHADE = cluster shade, SVAR = sum variance, VAR = variance.

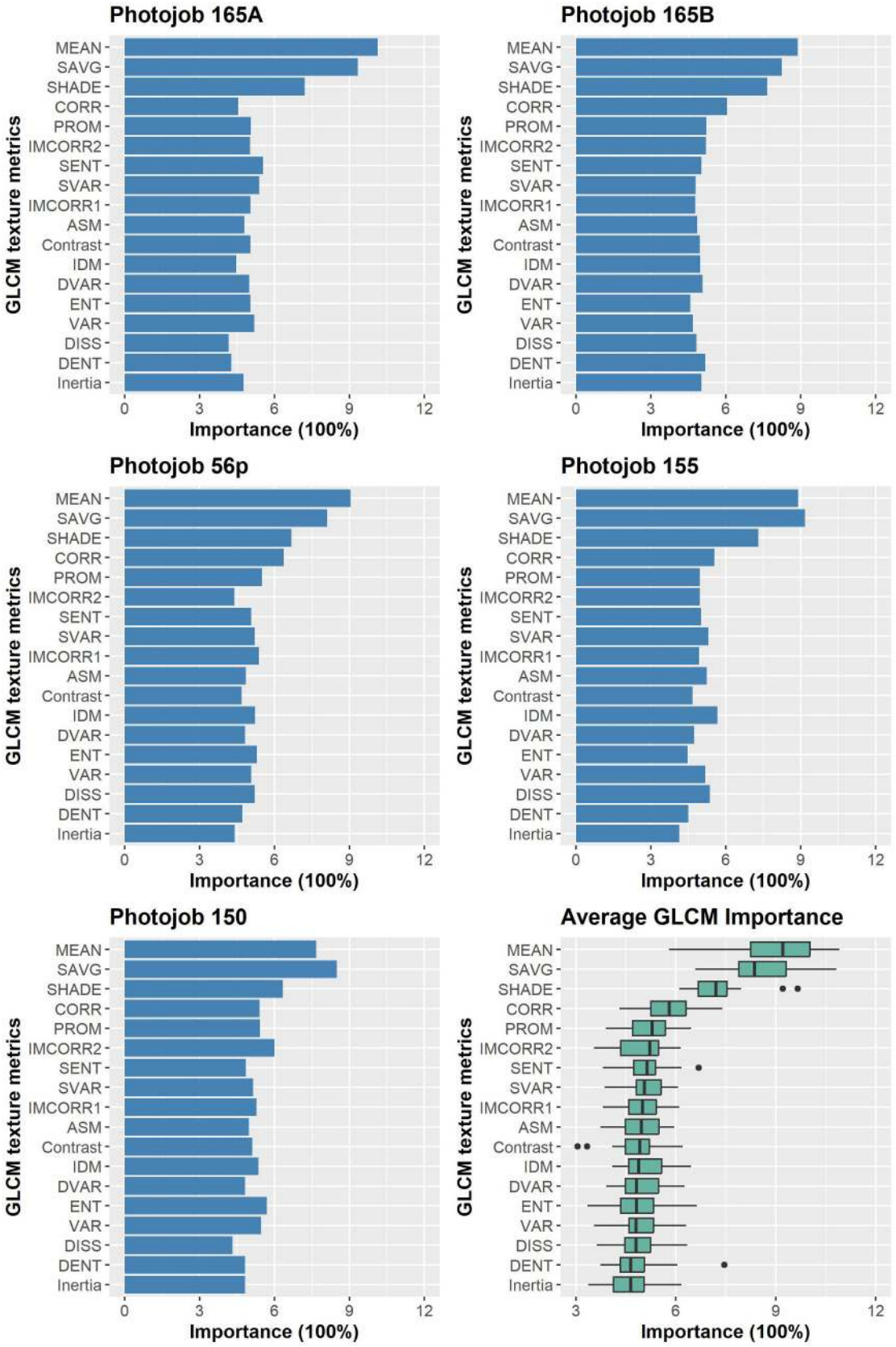

Fig. A.4. Variable importance of GLCM texture features for each photojob (Fig. 1) and on the bottom right a boxplot showing the average importance value of each GLCM feature and the maximum and minimum values. The GLCM features: ASM = angular second moment, Contrast, CORR = correlation, DENT = difference entropy, DISS = dissimilarity, DVAR = difference variance, ENT = Entropy, IDM = inverse difference moment, IMCORR1 = information measure of Corr. 1, IMCORR2 = information measure of Corr. 2, Inertia, MEAN = mean-difference-to-neighboring brightness, PROM = cluster prominence, SAVG = Sum Average, SENT = sum entropy, SHADE = cluster shade, SVAR = sum variance, VAR = variance.

Appendix B. Supplementary data

Supplementary data to this article can be found online at https://doi.org/10.1016/j.ecoinf.2024.102590.

References

Abu, I.-O., Szantoi, Z., Brink, A., Robuchon, M., Thiel, M., 2021. Detecting cocoa plantations in Côte d'Ivoire and Ghana and their implications on protected areas. Ecol. Indic. 129, 107863 https://doi.org/10.1016/j.ecolind.2021.107863.

Achanta, R., Susstrunk, S., 2017. Superpixels and polygons using simple non-iterative clustering. In: Presented at the Proceedings of the IEEE Conference on Computer Vision and Pattern Recognition, pp. 4651–4660. https://doi.org/10.1109/CVPR.2017.520.

Alves de Oliveira, B.F., Bottino, M.J., Nobre, P., Nobre, C.A., 2021. Deforestation and climate change are projected to increase heat stress risk in the Brazilian Amazon. Commun. Earth Environ 2, 1–8. https://doi.org/10.1038/s43247-021-00275-8.

Bauer, M.E., 1975. The role of remote sensing in determining the distribution and yield of crops. In: Brady, N.C. (Ed.), Advances in Agronomy. Academic Press, pp. 271–304. https://doi.org/10.1016/S0065-2113(08)70012-9.

Belgiu, M., Drăguţ, L., 2016. Random forest in remote sensing: a review of applications and future directions. ISPRS J. Photogramm. Remote Sens. 114, 24–31. https://doi.org/10.1016/j.isprsjprs.2016.01.011.

Blaschke, T., 2010. Object based image analysis for remote sensing. ISPRS J. Photogramm. Remote Sens. 65, 2–16. https://doi.org/10.1016/j.isprsjprs.2009.06.004.

Boothroyd, R.J., Williams, R.D., Hoey, T.B., Barrett, B., Prasojo, O.A., 2021. Applications of Google earth engine in fluvial geomorphology for detecting river channel change. WIREs Water 8, e21496. https://doi.org/10.1002/wat2.1496.

Breiman, L., 2001. Random forests. Mach. Learn. 45, 5–32. https://doi.org/10.1023/A:1010933404324.

Cardille, J.A., Crowley, M.A., Saah, D., Clinton, N.E. (Eds.), 2024. Cloud-Based Remote Sensing with Google Earth Engine: Fundamentals and Applications. Springer International Publishing, Cham. https://doi.org/10.1007/978-3-031-26588-4.

Coetsee, C., Botha, J., Case, M.F., Manganyi, A., Siebert, F., 2023. The hard lives of trees in African savanna—even without elephants. Austral. Ecol. 48, 532–551. https://doi.org/10.1111/aec.13283.

Conners, R.W., Trivedi, M.M., Harlow, C.A., 1984. Segmentation of a high-resolution urban scene using texture operators. Comp. Vision Graph. Image Proc. 25, 273–310. https://doi.org/10.1016/0734-189X(84)90197-X.

Das, A.A., Thaker, M., Coetsee, C., Slotow, R., Vanak, A.T., 2022. The importance of history in understanding large tree mortality in African savannas. Ecography 2022. https://doi.org/10.1111/ecog.06012.

Drăguţ, L., Schauppenlehner, T., Muhar, A., Strobl, J., Blaschke, T., 2009. Optimization of scale and parametrization for terrain segmentation: an application to soil-landscape modeling. Comput. Geosci. 35, 1875–1883. https://doi.org/10.1016/j.cageo.2008.10.008.

Du Toit, J.T., Rogers, K.H., Biggs, H.C., 2003. The Kruger Experience: Ecology and Management of Savanna Heterogeneity. Island Press.

Eckhardt, H.C., van Wilgen, B.W., Biggs, H.C., 2000. Trends in woody vegetation cover in the Kruger National Park, South Africa, between 1940 and 1998. Afr. J. Ecol. 38, 108–115. https://doi.org/10.1046/j.1365-2028.2000.00217.x.

Fensham, R.J., Fairfax, R.J., 2002. Aerial photography for assessing vegetation change: a review of applications and the relevance of findings for Australian vegetation history. Aust. J. Bot. 50 https://doi.org/10.1071/BT01032.

Fensham, R.J., Fairfax, R.J., Holman, J.E., Whitehead, P.J., 2002. Quantitative assessment of vegetation structural attributes from aerial photography. Int. J. Remote Sens. 23, 2293–2317. https://doi.org/10.1080/01431160110106050.

Ferreira, S.M., Greaver, C., Simms, C., 2017. Elephant population growth in Kruger National Park, South Africa, under a landscape management approach. Koedoe 59, 6. https://doi.org/10.4102/koedoe.v59i1.1427.

Frake, A.N., Peter, B.G., Walker, E.D., Messina, J.P., 2020. Leveraging big data for public health: mapping malaria vector suitability in Malawi with Google earth engine. PLoS One 15, e0235697. https://doi.org/10.1371/journal.pone.0235697.

Gertenbach, W.P.D., 1980. Rainfall patterns in the Kruger National Park. Koedoe 23, 35–43. https://doi.org/10.4102/koedoe.v23i1.634.

Gertenbach, W.P.D., 1983. Landscapes of the Kruger National Park. Koedoe 26, 9–121. https://doi.org/10.4102/koedoe.v26i1.591.

Godfray, H.C.J., Beddington, J.R., Crute, I.R., Haddad, L., Lawrence, D., Muir, J.F., Pretty, J., Robinson, S., Thomas, S.M., Toulmin, C., 2010. Food security: the challenge of feeding 9 billion people. Science 327, 812–818. https://doi.org/10.1126/science.1185383.

Hammond, T.O., Verbyla, D.L., 1996. Optimistic bias in classification accuracy assessment. Int. J. Remote Sens. 17, 1261–1266. https://doi.org/10.1080/01431169608949085.

Hansen, M.C., Potapov, P.V., Moore, R., Hancher, M., Turubanova, S.A., Tyukavina, A., Thau, D., Stehman, S.V., Goetz, S.J., Loveland, T.R., Kommareddy, A., Egorov, A., Chini, L., Justice, C.O., Townshend, J.R.G., 2013. High-resolution global maps of 21st-century Forest cover change. Science 342, 850–853. https://doi.org/10.1126/science.1244693.

Haralick, R.M., Shanmugam, K., Dinstein, I., 1973. Textural features for image classification. IEEE Trans. Syst. Man Cybern. SMC-3, 610–621. https://doi.org/10.1109/TSMC.1973.4309314.

Hassan, Z., Shabbir, R., Ahmad, S.S., Malik, A.H., Aziz, N., Butt, A., Erum, S., 2016. Dynamics of land use and land cover change (LULCC) using geospatial techniques: a case study of Islamabad Pakistan. SpringerPlus 5, 812. https://doi.org/10.1186/s40064-016-2414-z.

Hay, G.J., Castilla, G., 2008. Geographic object-based image analysis (GEOBIA): A new name for a new discipline. In: Blaschke, T., Lang, S., Hay, Geoffrey J. (Eds.), Object-Based Image Analysis: Spatial Concepts for Knowledge-Driven Remote Sensing Applications, Lecture Notes in Geoinformation and Cartography. Springer, Berlin, Heidelberg, pp. 75–89. https://doi.org/10.1007/978-3-540-77058-9_4.

Jagannathan, J., Divya, C., 2021. Deep learning for the prediction and classification of land use and land cover changes using deep convolutional neural network. Eco. Inform. 65, 101412 https://doi.org/10.1016/j.ecoinf.2021.101412.

Joshi, A.R., Dinerstein, E., Wikramanayake, E., Anderson, M.L., Olson, D., Jones, B.S., Seidensticker, J., Lumpkin, S., Hansen, M.C., Sizer, N.C., Davis, C.L., Palminteri, S., Hahn, N.R., 2016. Tracking changes and preventing loss in critical tiger habitat. Sci. Adv. 2, e1501675 https://doi.org/10.1126/sciadv.1501675.

Kadmon, R., Harari-Kremer, R., 1999. Studying long-term vegetation dynamics using digital processing of historical aerial photographs. Remote Sens. Environ. 68, 164–176. https://doi.org/10.1016/S0034-4257(98)00109-6.

Kayitesi, N.M., Guzha, A.C., Mariethoz, G., 2022. Impacts of land use land cover change and climate change on river hydro-morphology- a review of research studies in tropical regions. J. Hydrol. 615, 128702 https://doi.org/10.1016/j.jhydrol.2022.128702.

Knoop, W.T., Walker, B.H., 1985. Interactions of Woody and Herbaceous vegetation in a Southern African Savanna. J. Ecol. 73, 235–253. https://doi.org/10.2307/2259780.

Laurance, W.F., Sayer, J., Cassman, K.G., 2014. Agricultural expansion and its impacts on tropical nature. Trends Ecol. Evol. 29, 107–116. https://doi.org/10.1016/j.tree.2013.12.001.

Levick, S.R., Rogers, K.H., 2011. Context-dependent vegetation dynamics in an African savanna. Landsc. Ecol. 26, 515–528. https://doi.org/10.1007/s10980-011-9578-2.

Lillesand, T.M., Kiefer, R.W., Chipman, J.W., 2004. Remote Sensing and Image Interpretation. Wiley.

MacFadyen, S., Zambatis, N., Van Teeffelen, A.J.A., Hui, C., 2018. Long-term rainfall regression surfaces for the Kruger National Park, South Africa: a spatio-temporal review of patterns from 1981 to 2015. Int. J. Climatol. 38, 2506–2519. https://doi.org/10.1002/joc.5394.

Millard, K., Richardson, M., 2015. On the importance of training data sample selection in random forest image classification: a case study in peatland ecosystem mapping. Remote Sens. 7, 8489–8515. https://doi.org/10.3390/rs70708489.

Morgan, J.L., Gergel, S.E., 2010. Quantifying historic landscape heterogeneity from aerial photographs using object-based analysis. Landsc. Ecol. 25, 985–998. https://doi.org/10.1007/s10980-010-9474-1.

Munteanu, C., Kamp, J., Nita, M.D., Klein, N., Kraemer, B.M., Müller, D., Koshkina, A., Prishchepov, A.V., Kuemmerle, T., 2020. Cold war spy satellite images reveal long-term declines of a philopatric keystone species in response to cropland expansion. Proc. R. Soc. B Biol. Sci. 287, 20192897. https://doi.org/10.1098/rspb.2019.2897.

Munyati, C., Sinthumule, N.I., 2016. Change in woody cover at representative sites in the Kruger National Park, South Africa, based on historical imagery. SpringerPlus 5, 1417. https://doi.org/10.1186/s40064-016-3036-1.

Pacheco Quevedo, R., Velastegui-Montoya, A., Montalván-Burbano, N., Morante-Carballo, F., Korup, O., Daleles Rennó, C., 2023. Land use and land cover as a conditioning factor in landslide susceptibility: a literature review. Landslides 20, 967–982. https://doi.org/10.1007/s10346-022-02020-4.

Park, Y., Guldmann, J.-M., 2020. Measuring continuous landscape patterns with gray-level co-occurrence matrix (GLCM) indices: an alternative to patch metrics? Ecol. Indic. 109, 105802 https://doi.org/10.1016/j.ecolind.2019.105802.

Powers, R.P., Jetz, W., 2019. Global habitat loss and extinction risk of terrestrial vertebrates under future land-use-change scenarios. Nat. Clim. Chang. 9, 323–329. https://doi.org/10.1038/s41558-019-0406-z.

Priyanka, Kumar D., 2020. Feature extraction and selection of kidney ultrasound images using GLCM and PCA. In: Procedia Computer Science, International Conference on Computational Intelligence and Data Science, 167, pp. 1722–1731. https://doi.org/10.1016/j.procs.2020.03.382.

QGIS Development Team, 2023. QGIS Geographic Information System.

Radoux, J., Defourny, P., Bogaert, P., 2008. Comparison of pixel-and object-based sampling strategies for thematic accuracy assessment. In: GEOBIA 2008-Pixels, Objects, Intelligence, pp. 5–8.

Ren, X., Malik, J., 2003. Learning a classification model for segmentation. In: Proceedings Ninth IEEE International Conference on Computer Vision. Presented at the ICCV 2003: 9th International Conference on Computer Vision, vol. 1. IEEE, Nice, France, pp. 10–17. https://doi.org/10.1109/ICCV.2003.1238308.

Rodriguez-Galiano, V.F., Ghimire, B., Rogan, J., Chica-Olmo, M., Rigol-Sanchez, J.P., 2012. An assessment of the effectiveness of a random forest classifier for land-cover classification. ISPRS J. Photogramm. Remote Sens. 67, 93–104. https://doi.org/10.1016/j.isprsjprs.2011.11.002.

Scholes, R.J., Walker, B.H., 1993. An African Savanna: Synthesis of the Nylsvley Study, Cambridge Studies in Applied Ecology and Resource Management. Cambridge University Press, Cambridge. https://doi.org/10.1017/CBO9780511565472.

Scholtz, R., Kiker, G.A., Smit, I.P.J., Venter, F.J., 2014. Identifying drivers that influence the spatial distribution of woody vegetation in Kruger National Park, South Africa. Ecosphere 5, art71. https://doi.org/10.1890/ES14-00034.1.

Sealey, K.S., Binder, P.-M., Burch, R.K., 2018. Financial credit drives urban land-use change in the United States. Anthropocene 21, 42–51. https://doi.org/10.1016/j.ancene.2018.01.002.

Shafeian, E., Fassnacht, F.E., Latifi, H., 2021. Mapping fractional woody cover in an extensive semi-arid woodland area at different spatial grains with Sentinel-2 and very high-resolution data. Int. J. Appl. Earth Obs. Geoinf. 105, 102621 https://doi.org/10.1016/j.jag.2021.102621.

Smit, I.P.J., Asner, G.P., Govender, N., Kennedy-Bowdoin, T., Knapp, D.E., Jacobson, J., 2010. Effects of fire on woody vegetation structure in African savanna. Ecol. Appl. 20, 1865–1875. https://doi.org/10.1890/09-0929.1.

Smit, I.P.J., Riddell, E.S., Cullum, C., Petersen, R., 2013a. Kruger National Park research supersites: establishing long-term research sites for cross-disciplinary, multiscaled learning. Koedoe 55, 1–7. https://doi.org/10.4102/koedoe.v55i1.1107.

Smit, I.P.J., Smit, C.F., Govender, N., van der Linde, M., MacFadyen, S., 2013b. Rainfall, geology and landscape position generate large-scale spatiotemporal fire pattern heterogeneity in an African savanna. Ecography 36, 447–459. https://doi.org/10.1111/j.1600-0587.2012.07555.x.

Soga, M., Gaston, K.J., 2018. Shifting baseline syndrome: causes, consequences, and implications. Front. Ecol. Environ. 16, 222–230. https://doi.org/10.1002/fee.1794.

Stevenson-Hamilton, J., 1993. South African Eden: The Kruger National Park, 1902–1946, 1993rd ed. Struik, Cape Town.

Tassi, A., Vizzari, M., 2020. Object-oriented LULC classification in Google earth engine combining SNIC, GLCM, and machine learning algorithms. Remote Sens. 12, 3776. https://doi.org/10.3390/rs12223776.

Tassi, A., Gigante, D., Modica, G., Di Martino, L., Vizzari, M., 2021. Pixel- vs. object-based Landsat 8 data classification in Google earth engine using random Forest: the case study of Maiella National Park. Remote Sens. 13, 2299. https://doi.org/10.3390/rs13122299.

Trabucco, A., Zomer, R., 2014. Influence of Aridity on Vegetation [WWW Document]. https://doi.org/10.2499/9780896298460_23.

United Nations Convention to Combat Desertification, 2022. Global Land Outlook, 2nd edition. UNCCD, Bonn.

Urban, M., Heckel, K., Berger, C., Schratz, P., Smit, I.P.J., Strydom, T., Baade, J., Schmullius, C., 2020. Woody cover mapping in the savanna ecosystem of the Kruger National Park using Sentinel-1 C-band time series data. Koedoe 62, 1–6. https://doi.org/10.4102/koedoe.v62i1.1621.

Verburg, P.H., Neumann, K., Nol, L., 2011. Challenges in using land use and land cover data for global change studies. Glob. Chang. Biol. 17, 974–989. https://doi.org/10.1111/j.1365-2486.2010.02307.x.

Vogels, M.F.A., de Jong, S.M., Sterk, G., Addink, E.A., 2017. Agricultural cropland mapping using black-and-white aerial photography, object-based image analysis and random forests. Int. J. Appl. Earth Obs. Geoinf. 54, 114–123. https://doi.org/10.1016/j.jag.2016.09.003.

Whiteside, T.G., Boggs, G.S., Maier, S.W., 2011. Comparing object-based and pixel-based classifications for mapping savannas. Int. J. Appl. Earth Obs. Geoinf. 13, 884–893. https://doi.org/10.1016/j.jag.2011.06.008.

Whiteside, T.G., Esparon, A.J., Bartolo, R.E., 2020. A semi-automated approach for quantitative mapping of woody cover from historical time series aerial photography and satellite imagery. Eco. Inform. 55, 101012 https://doi.org/10.1016/j.ecoinf.2019.101012.

Wolhuter, H., 2010. Memories of a Game Ranger. Protea Book House.

Wright, R., 1973. Remote sensing techniques in vegetation mapping—a review of some uses and limitations. Trans. Botanic. Soc. Edinburgh 42, 69–81. https://doi.org/10.1080/03746607308685262.

Wulder, M., 1998. Optical remote-sensing techniques for the assessment of forest inventory and biophysical parameters. Progr. Phys. Geogr. Earth Environ. 22, 449–476. https://doi.org/10.1177/030913339802200402.

Yang, X., Crews, K.A., 2019. Fractional Woody cover mapping of Texas savanna at Landsat scale. Land 8, 9. https://doi.org/10.3390/land8010009.

Yang, D., Kanae, S., Oki, T., Koike, T., Musiake, K., 2003. Global potential soil erosion with reference to land use and climate changes. Hydrol. Process. 17, 2913–2928. https://doi.org/10.1002/hyp.1441.

Yang, X., Tridandapani, S., Beitler, J.J., Yu, D.S., Yoshida, E.J., Curran, W.J., Liu, T., 2012. Ultrasound GLCM texture analysis of radiation-induced parotid-gland injury in head-and-neck cancer radiotherapy: an in vivo study of late toxicity. Med. Phys. 39, 5732–5739. https://doi.org/10.1118/1.4747526.

Zambatis, N., 2003. Determinants of Grass Production and Composition in the Kruger National Park (Thesis).